Hindawi Publishing Corporation
Journal of Nanomaterials
Volume 2015, Article ID 298692, 7 pages
http://dx.doi.org/10.1155/2015/298692

Research Article

Size-Dependent Optical Properties of Nanoscale and Bulk Long Persistent Phosphor $SrAl_2O_4:Eu^{2+}$, Dy^{3+}

Xiaoxia Duan,[1] Lixin Yi,[2] Xiqing Zhang,[2] and Shihua Huang[2]

[1]*Department of Chemistry, School of Science, Beijing Jiaotong University, Beijing 100044, China*
[2]*Key Laboratory of Luminescence and Optical Information, Ministry of Education, Institute of Optoelectronic Technology, Beijing Jiaotong University, Beijing 100044, China*

Correspondence should be addressed to Xiaoxia Duan; xxduan@bjtu.edu.cn

Received 27 December 2014; Revised 13 March 2015; Accepted 14 March 2015

Academic Editor: Yong Zhu

Nanoscale long persistent phosphor $SrAl_2O_4:Eu^{2+}$, Dy^{3+} was prepared by autocombustion of citrate gel. The energy level shift of activator Eu^{2+} and coactivator Dy^{3+} was analyzed according to the emission and the excitation spectra. The band gap change of $SrAl_2O_4$ and the resulting trap depth change with particle size were discussed on the basis of analyzing the visible spectra, the vacuum ultraviolet (VUV) excitation spectra, and the thermoluminescence (TL) spectra. The fluorescence quenching and the shallow traps originating from surface adsorption or surface defects explain the weak initial persistent phosphorescence and the fast phosphorescence decay in nanometer $SrAl_2O_4:Eu^{2+}$, Dy^{3+}. It is confirmed that energy level, band gap, trap depth, defect, and surface adsorption are deeply related with each other in this nanoscale long persistent phosphor.

1. Introduction

The theoretical model of long persistent phosphor is generally composed of three parts: matrix lattice, emitters, and traps [1], among which, emitters and traps are named as activator centers [2]. Emitters are centers capable of emitting radiation after being excited. Traps can be lattice defects originating from material itself or coactivator [2]. They usually do not emit radiation but store excitation energy and release it gradually to the emitters because of thermal or other physical stimulations. The trap energy level should be at a suitable position in forbidden band. Thus the emission wavelength of a persistent phosphor is mainly determined by the emission centers; the afterglow intensity and decay time are determined by the trap state (type and distribution) [1].

Long persistent phosphors have been rapidly developed in the past decades. Many of them have already been commercialized and are being widely used as night-vision materials in various important fields (e.g., security signs, emergency route signs, traffic signage, dials and displays, medical diagnostics, and optical probes in bioimaging) [3–11].

Among all the works, most researchers pay more attention to finding some new materials with long afterglow time and stability. In fact, to improve the original properties and to study the persistent luminescence mechanisms are also very important [11–13]. Traps play very important role in long persistent phosphor. Trap depth is defined as the energy difference between the bottom of the conduction band and the trap energy level. The band gap of matrix lattice increases because of quantum confining effect when the particle size is minimized to nanometer, but the trap energy level is localized. So, theoretically the trap depth will increase. In view of this, it is predicted that the long afterglow properties will get better if the particle size is minimized to nanometer.

In this work, nanoscale and bulk long persistent phosphor were prepared. The size-dependent spectroscopy properties were studied systematically. This is very important for deeply exploring the persistent luminescence mechanism.

2. Experimental

Nanoscale and bulk $SrAl_2O_4:Eu^{2+}$, Dy^{3+} were prepared, respectively, with the method described previously [14]. The solution was controlled at pH 7. The quantity of citric acid was denoted by formula $n_{CA}/n_M{}^{n+} = 2$, where n_{CA} is

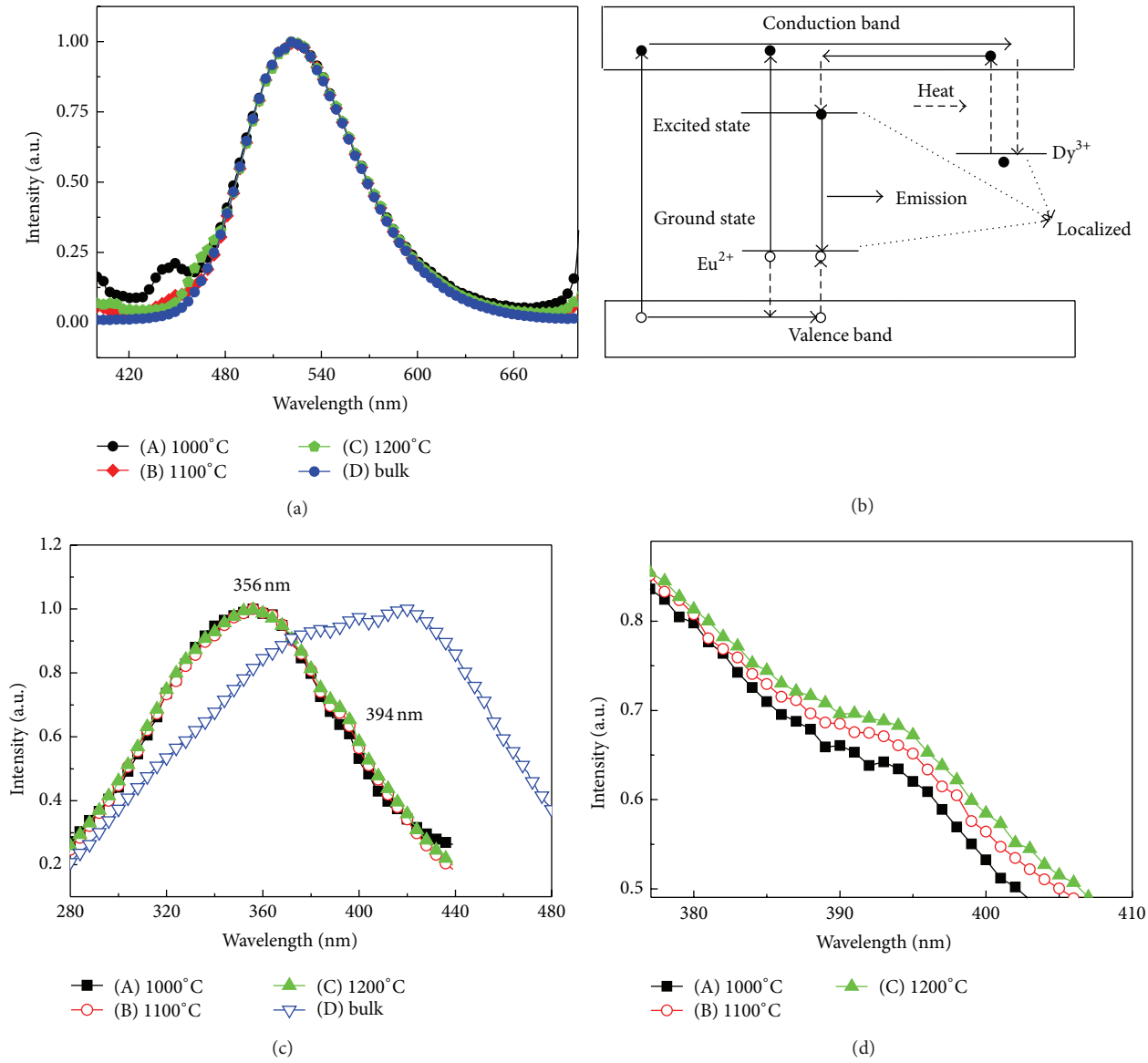

FIGURE 1: Emission spectra and excitation spectra. (a) Emission spectra of nanoscale and bulk $SrAl_2O_4$:Eu^{2+}, Dy^{3+}, λ_{Ex} = 360 nm. (b) Afterglow mechanism of long persistent phosphor. (c) Excitation spectra of nanoscale and bulk $SrAl_2O_4$:Eu^{2+}, Dy^{3+}, λ_{Em} = 520 nm. (d) The enlarged drawing of excitation spectra of nanoscale $SrAl_2O_4$:Eu^{2+}, Dy^{3+} in the vicinity of 394 nm, λ_{Em} = 520 nm. (A), (B), and (C) correspond, respectively, to the nanomaterial prepared at 1000°C, 1100°C, and 1200°C and (D) corresponds to the bulk material. The particle size is $R_A < R_B < R_C < R_D$.

the mole number of citric acid and n_M^{n+} is the mole number of all the metal ion. The sintering temperature was separately set at 900°C, 1000°C, 1100°C, and 1200°C. The particle size of the obtained nanomaterial increases with the sintering temperature.

The emission spectra of the samples were measured by using INS-150-122B CCD spectrometer with a Xe lamp as light source. The excitation spectra were measured using a Flurolog-3 fluorescent spectrometer. The VUV excitation spectra were measured with a vacuum ultraviolet spectrometer. The TL glow curves of all the samples were carried out with FJ-4272 thermoluminescence instrument. The surface adsorption was analyzed by using GX Fourier transform infrared (FTIR) spectrometer. The afterglow decay was analyzed by using Keithley 2410 and optical power meter. All the measurements were conducted at room temperature.

3. Results and Discussion

3.1. Emission Spectra and Excitation Spectra. Figure 1(a) shows the emission spectra of nanometer and bulk $SrAl_2O_4$:Eu^{2+}, Dy^{3+}. The exciting wavelength is 360 nm. (A), (B), and (C) refer, respectively, to nanometer material prepared at 1000°C, 1100°C, and 1200°C and (D) refers

to the bulk material. The particle size is listed as follows: $R_A < R_B < R_C < R_D$. The emission at 522 nm is attributed to $4f^6 5d^1$-$4f^7$ transition of Eu^{2+}. The emission peaks of nanoscale $SrAl_2O_4$:Eu^{2+}, Dy^{3+} are essentially coincident with that of the bulk phosphor. 5d electrons are exposed out of Eu^{2+}. Generally speaking, the energy level of rare earth ions is strongly localized. This is fit for activators (Eu^{2+}) and traps (Dy^{3+}) listed in Figure 1(b). The energy level difference between the lowest excited state $4f^6 5d^1$ and the ground state $4f^7$ does not change clearly when the particle size is reduced to nanometer scale, so the peak wavelength remains motionless.

The excitation spectra corresponding to the emission spectra in Figure 1(a) are shown in Figure 1(c). The detection wavelength was set at 520 nm. Compared to the emission spectra, the regularity of excitation spectra shows great difference. Firstly, the excitation spectra of the nanoparticles show obvious blue shift. Next, it can be seen in Figure 1(d) that the intensity value at 394 nm decreases with particle size decreasing. The emission intensity ratio ($\beta_1 = I_{356\,nm}/I_{394\,nm}$) increases with particle size decreasing although the excitation spectra of nanoscale $SrAl_2O_4$:Eu^{2+}, Dy^{3+} do not show obvious blue shift compared to the bigger nanoparticles. Besides, the luminous intensity of the nanoparticles inclines to decrease from 356 nm to 420 nm, but the bulk material inclines to increase in this range. All these three aspects indicate that the phosphor with the smaller size inclines to absorb the shorter wavelength irradiation.

From the above analysis, it can be concluded that the two luminescence related energy levels of Eu^{2+} in $SrAl_2O_4$:Eu^{2+}, Dy^{3+} do not move clearly with particle size and crystal field has a greater influence on the higher excited state than on the lower excited state of emission center (activator here is Eu^{2+}). In $SrAl_2O_4$:Eu^{2+}, Dy^{3+}, the coactivator Dy^{3+} and the activator Eu^{2+} have similar electron shell structure and the trap level lies between the two luminescence related energy levels, so the trap level tends to lie in a relatively stable position. It can be deduced that the trap level provided by Dy^{3+} ions will not move up or down greatly with particle size decreasing (Figure 1(d)). This determines the trap level will be maintained at the original station when the particle size of $SrAl_2O_4$:Eu^{2+}, Dy^{3+} decreases to nanometer scale.

3.2. VUV Excitation Spectra and Band Gap. Figure 2(a) shows the VUV excitation spectra of nanometer and bulk $SrAl_2O_4$:Eu^{2+}, Dy^{3+}. Lines (A), (B), (C), and (D), respectively, refer to the nanometer samples prepared at 900°C, 1000°C, 1100°C, and 1200°C. Line (E) refers to the bulk material. The band gap of host crystal $SrAl_2O_4$ is 6.52 eV, and the corresponding absorption edge should be at about 190 nm. It can be seen from Figure 2(a) that the band edges locate just near 190 nm. Here, the detection wavelength was set at 520 nm, which is the characteristic emission peak of Eu^{2+} ion. This means that the energy can be well transferred between the emission centers (Eu^{2+}) and the host crystal ($SrAl_2O_4$) [13, 15, 16]. The VUV excitation spectra actually reflect the light absorption of host crystal $SrAl_2O_4$ when detecting 520 nm of emission.

For bulk semiconductor, the energy of the valence band and the conduction band distributes continuously. Band gap width is the distance between the valence band and the conduction band. For nanometer semiconductor, the energy of the valence band and the conduction band is no longer continuous and the band gap width increases when the particle size decreases (Figure 2(c)), which can be seen in Figure 2(b) (the enlarged picture of the band edge between 168 nm and 180 nm in Figure 2(a)). The VUV excitation spectra of the nanometer $SrAl_2O_4$:Eu^{2+}, Dy^{3+} shift to the shorter wavelength compared to that of the bulk one. At the same time, the spectra of the nanoparticles shift to the shorter wavelength one by one with particle size decreasing from (B) to (E). Besides, there are two peaks at $\lambda_1 = 168$ nm and $\lambda_2 = 180$ nm in VUV excitation spectra. It is clear that the ratio $\beta_2 = I_{168\,nm}/I_{180\,nm}$ gets bigger and bigger with particle size decreasing from (A) to (E). This novel phenomenon indicates that the shorter wavelength absorption plays more and more important role when the particle size decreases. Therefore, it can be concluded that nanoscale $SrAl_2O_4$ should have wider band gap than the bulk one and the band gap inclines to increase with particle size decreasing.

3.3. Thermoluminescence Spectra and Trap Depth. According to the above analysis, the band gap of the nanoscale $SrAl_2O_4$ is wider than that of the bulk one. In addition, it has been mentioned in Section 3.1 that the traps energy level provided by Dy^{3+} will not shift greatly with particle size decreasing. It can be deduced furtherly that the nanoscale $SrAl_2O_4$:Eu^{2+}, Dy^{3+} has deeper traps than the bulk one. This is so-called quantum effect.

In order to find out what change has happened to the traps with particle size decreasing, TL spectra were measured after the samples were irradiated for 2 minutes by UV lamp (Figure 3). (A), (B), and (C), respectively, correspond to nanometer $SrAl_2O_4$:Eu^{2+}, Dy^{3+} prepared at 900°C, 1000°C, and 1100°C and (D) corresponds to bulk $SrAl_2O_4$:Eu^{2+}, Dy^{3+}. Each temperature peak in TL spectra corresponds to one kind of electron trap. Usually, the trap depth can be calculated according to Chen's equation [17] based on the peak temperature T_m and the shape of the TL curve. One has

$$
\begin{aligned}
E &= \frac{c_\tau k T_m^{\,2}}{\tau} - b_\tau 2kT_m,\\
c_\tau &= 1.51 + 3\left(\mu_g - 0.42\right),\\
b_\tau &= 1.58 + 4.52\left(\mu_g - 0.42\right),\\
\tau &= T_m - T_1,\\
\delta &= T_2 - T_m,\\
\omega &= T_2 - T_1,\\
\mu_g &= \frac{\delta}{\omega},
\end{aligned}
\tag{1}
$$

where T_1, T_m, and T_2 represent the temperature of half intensity at low-temperature side, peak temperature, and temperature of half intensity at high-temperature side of TL peak, τ

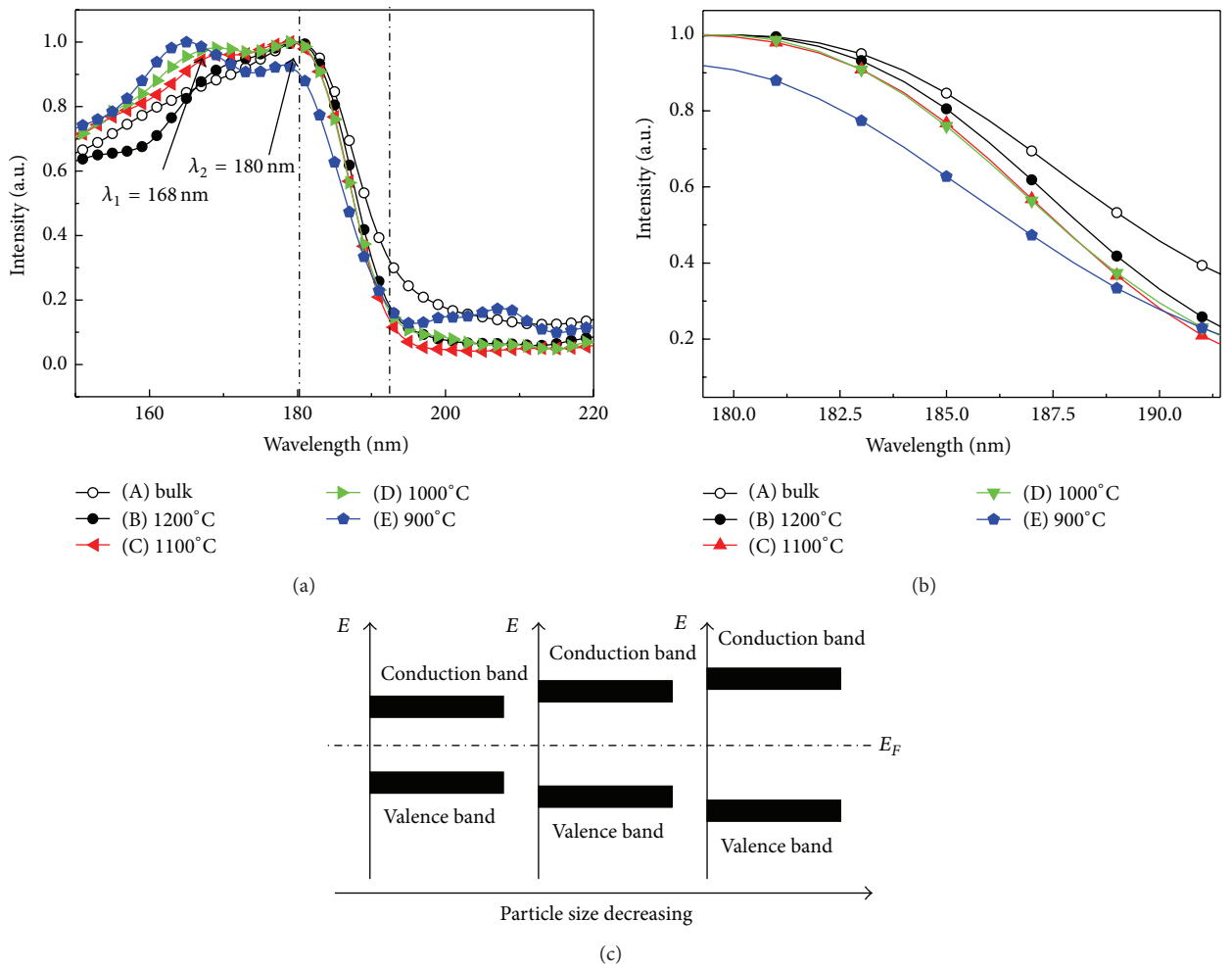

FIGURE 2: VUV excitation spectra and band gap. (a) VUV excitation spectra of nanoscale and bulk $SrAl_2O_4$:Eu^{2+}, Dy^{3+}, λ_{Em} = 520 nm. (b) Enlarged picture of VUV excitation spectra for nanoscale and bulk $SrAl_2O_4$:Eu^{2+}, Dy^{3+}, λ_{Em} = 520 nm. (c) Relationship between band gap and particle size of nanoscale semiconductor.

is the left half width, δ is the right half width, ω is the total half intensity width, k is Boltzmann's constant, and μ_g is the symmetry factor.

As shown in Figure 3(a), curve (A) has only one weak peak at about 350 K, curve (B) or curve (D) has one strong asymmetric peak, and curve (C) has two peaks at 350 K and 400 K. But the above method has its own unavoidable drawbacks. It is only fit for individual peaks and is limited when the spectra overlap partially together. Here, the trap depths were estimated using equation $E = T_m/500$ [17, 18].

It is clear that sample (A) has only one kind of shallow trap because it has only one weak TL peak at low temperature between 300 K and 350 K. Figures 3(b), 3(c), and 3(d) are the Gauss fitted results of curve (B), curve (C), and curve (D) in Figure 3(a). All the Gauss fitted peaks match very well with the original peaks. The peak at 350 K is considered originating from traps related with surface vacancy in nanoparticle. The 350 K peak intensity in line (B) is much stronger than that in line (A) because the luminescence quenching originated by surface vacancy decreases with particle size increasing. The 375 K peak is considered originating from the traps deepened by quantum size effect of the surface vacancy. The peaks at 400 K in lines (C) and (D) are considered originating from the inner vacancy. Besides, the peak at the highest temperature 460 K must have something to do with Dy^{3+}.

It can be seen in Figures 3(c) and 3(d) that the higher temperature peak plays more and more important role with particle size increasing. This can be deduced from the peak area. According to Urbach model $E = T_m/500$, the trap depth at 350 K, 375 K, 400 K, and 460 K is, respectively, 0.70 eV, 0.75 eV, 0.80 eV, and 0.92 eV. In bulk material, the traps were provided by inner vacancy and Dy^{3+}. This is beyond all doubt. In nanoscale $SrAl_2O_4$:Eu^{2+}, Dy^{3+}, there should have been Dy^{3+} related peak at higher temperature according to the deduction at the beginning in Section 3.3. In fact, the electrons in this trap perhaps relax quickly to the surface state without giving emission. This supposed deep trap did not and will not appear in thermoluminescence spectra.

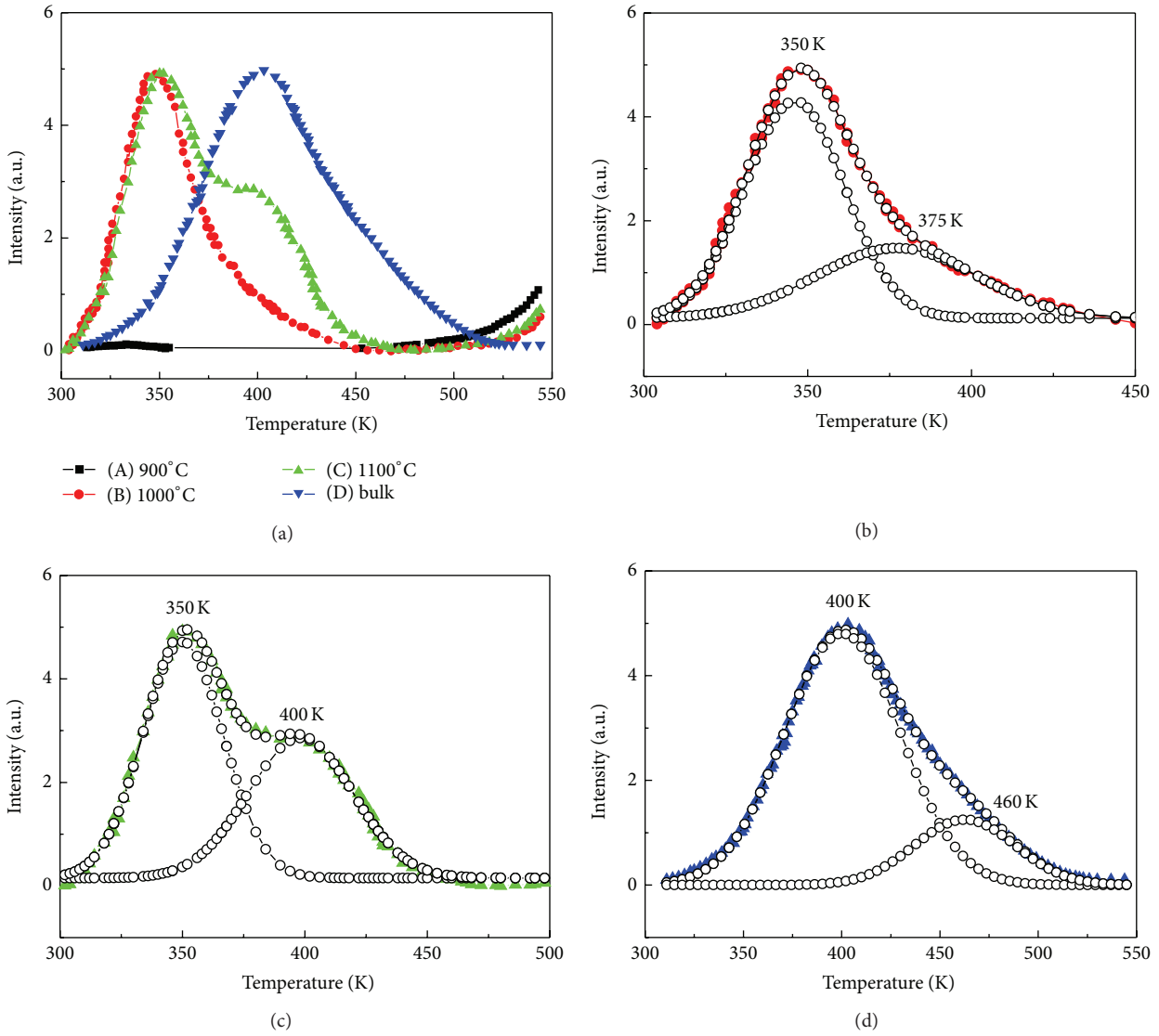

FIGURE 3: Size-dependent thermoluminescence spectra of $SrAl_2O_4$:Eu^{2+}, Dy^{2+} phosphors. (a) Thermoluminescence spectra of nanoscale $SrAl_2O_4$:Eu^{2+}, Dy^{2+} prepared by sol-gel method at 900°C (A), 1000°C (B), and 1100°C (C) and bulk phosphors (D) prepared by solid-state reaction method. (b) The Gausses fitted result of curve (B) in (a). (c) The Gausses fitted result of curve (C) in (a). (d) The Gausses fitted result of curve (D) in (a). The solid circles, up triangles, and down triangles correspond to the measured value and the open circles correspond to the Gauss fitted data.

3.4. Surface Adsorption and Fluorescence Quenching [11]. Surface defects and surface adsorption are intrinsic and unavoidable in nanoscale materials. The surface adsorption was characterized with GX Fourier transform infrared spectrometer in order to confirm the relation between luminous intensity and surface state (Figure 4). There are many absorption peaks in the region of 400–900 cm^{-1}, which are ascribed to the monoclinic crystal structure of $SrAl_2O_4$. No difference is found between all the samples in this region. This indicates that all the prepared samples have the same crystal structure and this determines all the above comparing is effective. The most interesting thing is all the samples display excellent regularity in the other wave number range. The absorption peaks at 1632 cm^{-1} are due to C=O; the peaks at 1340–1572 cm^{-1} are due to the symmetric stretching vibration and the asymmetric stretching vibration of -CO_2-. The absorption peaks at 3460 cm^{-1} correspond to O-H bond adsorbed on the surface of nanoscale and bulk particles. It is very clear that the absorption intensity increases with particle size decreasing. This trend is consistent with surface effect of nanomaterials. In fact, all these adsorbed functional groups can also be regarded as special defects.

In general, the phonon energy originating from the interaction between the crystal field and luminescence center is very weak. The functional groups adsorbed on the surface are very light compared to rare earth ions. Their vibration

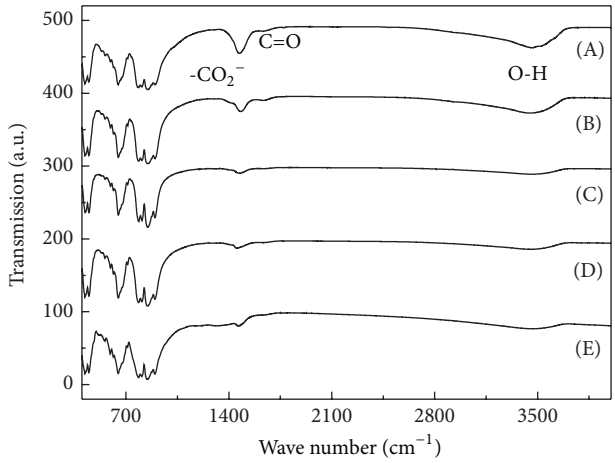

FIGURE 4: FTIR spectra of nanosized $SrAl_2O_4$:Eu^{2+}, Dy^{2+} phosphors prepared by sol-gel method at 900°C (A), 1000°C (B), 1100°C (C), and 1200°C (D) and bulk phosphors prepared by solid-state reaction method (E).

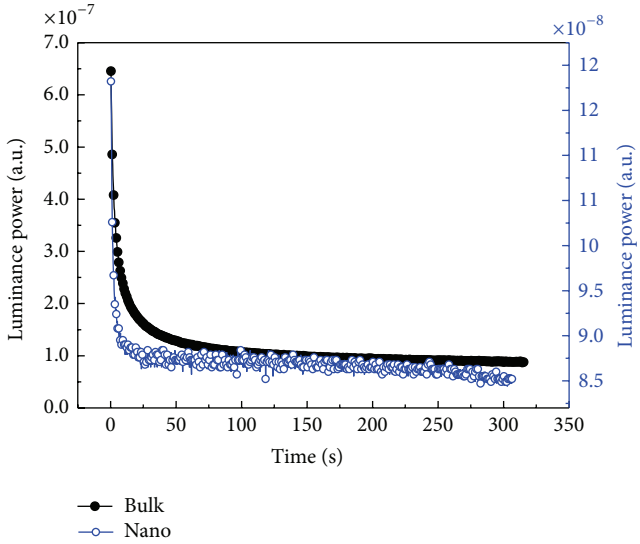

FIGURE 5: Decay curves at 520 nm emission peak of nanoscale (hollow circle) and bulk (solid circle) $SrAl_2O_4$:Eu^{2+}, Dy^{3+} phosphor. The right luminance power refers to nanoscale $SrAl_2O_4$:Eu^{2+}, Dy^{3+}, the left one refers to bulk $SrAl_2O_4$:Eu^{2+}, Dy^{3+}.

energy is very strong. The luminescent center near the surface couples with the vibration modes of those functional groups. The phonon energy provided by these vibration modes is relatively strong, so the electrons of luminescence center can easily relax to the lower energy level in nonradiative relaxation form and will not give out light. This process causes fluorescence quenching [19, 20] and this is just why the assumed deep traps did not work.

3.5. Long Persistent Phosphorescence and Decay Curve. According to the above analysis, deep traps play a leading role in bulk $SrAl_2O_4$:Eu^{2+}, Dy^{3+}. But for nanoscale $SrAl_2O_4$:Eu^{2+}, Dy^{3+}, the assumed deep traps originating from quantum size effect do not play their role due to the intrinsic surface defects and the unavoidable surface adsorptions. The electrons in the shallow traps are excited into the conduction band by thermal disturbance so easily that the long persistent luminescence decays quickly. Figure 5 is the luminous power versus time curve of nanoscale material prepared at 1100°C and the bulk material. The detected wavelength was set at the peak emission wavelength 520 nm. It is clear that the phosphorescence of nanoscale material decays much faster than that of the bulk one. In addition, the initial intensity of nanoscale long persistent phosphor is lower than that of the bulk phosphor and the final intensity of $SrAl_2O_4$:Eu^{2+}, Dy^{3+} tends to be much lower than that of the bulk $SrAl_2O_4$:Eu^{2+}, Dy^{3+}.

4. Conclusions

Nanoscale long persistent phosphors $SrAl_2O_4$:Eu^{2+}, Dy^{3+} with different size were prepared by autocombustion of citrate gelatin at 900°C, 1000°C, 1100°C, and 1200°C. The emission related energy levels of activator Eu^{2+} and the persistent luminescence related energy levels of coactivator Dy^{3+} do not change very clearly with particle size. The band gap of $SrAl_2O_4$ matrix crystal becomes wider and wider with particle size decreasing because of quantum effect. The smaller nanoparticles lead to the more serious surface adsorption and surface defects, which lead to nonradiative relaxation and fluorescence quenching. These factors are fatal for long persistent phosphor in nanoscale $SrAl_2O_4$:Eu^{2+}, Dy^{3+}. The deep traps originating from quantum size effect do not play their role because of surface effect. The shallow traps originating from surface defects give weak thermoluminescence or persistent phosphorescence. The afterglow of the nanoscale $SrAl_2O_4$:Eu^{2+}, Dy^{3+} decays faster than that of the bulk one.

Conflict of Interests

The authors declare that there is no conflict of interests regarding the publication of this paper.

Acknowledgments

The authors gratefully acknowledge the support from the Fundamental Research Funds for the Central Universities (no. 2013JBM099) and the National Natural Science Foundation of China (nos. 60977017 and 61275058).

References

[1] Z. W. Pan, Y. Y. Lu, and F. Liu, "Sunlight-activated long-persistent luminescence in the near-infrared from Cr^{3+}-doped zinc gallogermanates," *Nature Materials*, vol. 11, no. 1, pp. 58–63, 2012.

[2] W. M. Yen, S. Shionoya, and H. Yamamoto, *Phosphor Handbook*, CRC Press, 2007.

[3] Q. L. M. De Chermont, C. Chanéac, J. Seguin et al., "Nanoprobes with near-infrared persistent luminescence for *in vivo* imaging,"

Proceedings of the National Academy of Sciences of the United States of America, vol. 104, no. 22, pp. 9266–9271, 2007.

[4] L. C. V. Rodrigues, H. F. Brito, J. Hölsä, and M. Lastusaari, "Persistent luminescence behavior of materials doped with Eu^{2+} and Tb^{3+}," *Optical Materials Express*, vol. 2, no. 4, pp. 382–390, 2012.

[5] W. Zeng, Y. Wang, S. Han, W. Chen, G. Li, and Y. Wen, "Design, synthesis and characterization of a novel yellow long-persistent phosphor: $Ca_2BO_3Cl:Eu^{2+},Dy^{3+}$," *Journal of Materials Chemistry C*, vol. 1, no. 17, pp. 3004–3011, 2013.

[6] W. Chen and J. Zhang, "Using nanoparticles to enable simultaneous radiation and photodynamic therapies for cancer treatment," *Journal of Nanoscience and Nanotechnology*, vol. 6, no. 4, pp. 1159–1166, 2006.

[7] K. van den Eeckhout, P. F. Smet, and D. Poelman, "Persistent luminescence in Eu^{2+}-doped compounds: a review," *Materials*, vol. 3, no. 4, pp. 2536–2566, 2010.

[8] B.-Y. Wu, H.-F. Wang, J.-T. Chen, and X.-P. Yan, "Fluorescence resonance energy transfer inhibition assay for α-fetoprotein excreted during cancer cell growth using functionalized persistent luminescence nanoparticles," *Journal of the American Chemical Society*, vol. 133, no. 4, pp. 686–688, 2011.

[9] A. Abdukayum, J. T. Chen, Q. Zhao et al., "Functional near infrared-emitting Cr^{3+}/Pr^{3+} Co-doped zinc gallogermanate persistent luminescent nanoparticles with superlong afterglow for in vivo targeted bioimaging," *Journal of the American Society*, vol. 135, no. 38, pp. 14125–14133, 2013.

[10] M. Hepel and C. J. Zhong, "Persistent luminescence nanoparticles for diagnostics and imaging," in *Functional Nanoparticles for Bioanalysis, Nanomedicine, and Bioelectronic Devices*, vol. 2, pp. 1–25, American Chemical Society, Washington, DC, USA, 2012.

[11] G. F. Ju, Y. H. Hu, L. Chen, X. Wang, and Z. Mu, "Recent progress in Eu^{2+}-activated phosphate persistent phosphors," *Optical Materials*, vol. 36, no. 11, pp. 1920–1923, 2014.

[12] H. F. Brito, J. Hölsä, T. Laamanen, M. Lastusaari, M. Malkamäki, and L. C. V. Rodrigues, "Persistent luminescence mechanisms: human imagination at work," *Optical Materials Express*, vol. 2, no. 4, pp. 371–381, 2012.

[13] J. Hassinen, J. Hölsä, J. Niittykoski et al., "UV-VUV spectroscopy of rare earth doped persistent luminescence materials," *Optical Materials*, vol. 31, no. 12, pp. 1751–1754, 2009.

[14] X. X. Duan, S. H. Huang, F. T. You, Z. Xu, F. Teng, and L. Yi, "Electrooptical characteristics of nanoscale and bulk long persistent phosphor $SrAl_2O_4$: Eu, Dy," *Journal of Experimental Nanoscience*, vol. 4, no. 2, pp. 169–176, 2009.

[15] A. N. Belsky and J. C. Krupa, "Luminescence excitation mechanisms of rare earth doped phosphors in the VUV range," *Displays*, vol. 19, no. 4, pp. 185–196, 1999.

[16] M. Kamada, J. Murakami, and N. Ohno, "Excitation spectra of a long-persistent phosphor $SrAl_2O_4$:Eu, Dy in vacuum ultraviolet region," *Journal of Luminescence*, vol. 87–89, pp. 1042–1044, 2000.

[17] C. S. Shalgaonkar and A. V. Narlikar, "Review: a review of the recent methods for determining trap depth from glow curves," *Journal of Materials Science*, vol. 7, no. 12, pp. 1465–1471, 1972.

[18] R. Chen, Y. Hu, L. Chen, X. Wang, Y. Jin, and H. Wu, "Luminescent properties of a novel afterglow phosphor $Sr_3Al_2O_5Cl_2$: Eu^{2+}, Ce^{3+}," *Ceramics International*, vol. 40, no. 6, pp. 8229–8236, 2014.

[19] S. H. Huang, F. T. You, and H. S. Peng, "Influence of surface on spectroscopic properties of rare earth ions in nanocrystals," *Journal of Rare Earth*, vol. 25, no. 4, pp. 396–401, 2007.

[20] S. S. Pitale, S. K. Sharma, R. N. Dubey, M. S. Qureshi, and M. M. Malik, "Thermoluminescence glow curve analysis of UV irradiated long persistence CaS: Pr^{3+} phosphor through computerized glow curve deconvolution technique," *Nuclear Instruments and Methods in Physics Research, Section B: Beam Interactions with Materials and Atoms*, vol. 266, no. 9, pp. 2027–2034, 2008.